

Floquet-Hubbard bound states in the continuum

Giuseppe Della Valle* and Stefano Longhi

Dipartimento di Fisica and IFN-CNR, Politecnico di Milano, Piazza Leonardo da Vinci 32, I-20133 Milan, Italy

(Received 20 December 2013; revised manuscript received 24 February 2014; published 19 March 2014)

We theoretically demonstrate that a type of robust two-particle bound state embedded in the continuum (BIC), which we call Floquet-Hubbard (FH) BIC, can be induced in a homogeneous (i.e., defect-free) Hubbard semilattice by an intense oscillating electric field. While single-particle BIC states are fragile states that exist solely for specially tailored potentials, FH BIC states are found in a wide range of parameter space, do not require fulfillment of resonance conditions, and are thresholdless. Analytical results are derived in the high-frequency limit of field modulation by a multiple-time-scale asymptotic analysis of the ac-driven Hubbard Hamiltonian in the two-particle sector. A FH BIC mode basically corresponds to a molecular state, in which the two particles bind together, undergoing correlated tunneling on the lattice. Localization of the molecular state is induced by the external oscillating field, which effectively attracts the molecular state at the edge of the semi-infinite lattice. Our results can pave the way for the study and interpretation of strong-field phenomena in correlated-particles physics.

DOI: [10.1103/PhysRevB.89.115118](https://doi.org/10.1103/PhysRevB.89.115118)

PACS number(s): 03.65.Ge, 71.10.Fd, 71.27.+a

I. INTRODUCTION

The concept of a bound (i.e., normalizable) state embedded in a continuum (BIC) of energies dates back to the beginnings of quantum mechanics, with the pioneering work by von Neumann and Wigner [1]. BIC states are generally found in specially tailored potentials [2,3] or in systems where two or more resonances interfere [4,5]. In the latter case, the existence of the BIC states can be traced back to the original idea of Fano interference [6], which has been observed in a myriad of physical systems, from the classical to the quantum world [7–12] (see also Ref. [13] and references therein). BIC states also play an important role in quantum transport on the nanoscale with application to nanoelectronics [14] and spintronics [15]. Despite their ubiquity, BIC states are recognized as fragile states that generally decay into resonances by small perturbations [16], even though in some cases a certain robustness against hybridization into the continuum has been reported [17]. For these reasons, engineering of BIC states has been demonstrated only in special systems. As an example, photonic structures, allowing robust control of parameters, turned out to be very promising for the observation of BIC states [18–24], with potential impact on several applications, from large-field amplification and enhancement of optical nonlinearities to biosensing (as discussed in Ref. [18]). Interestingly, not only bulk BIC states [19] but also surface BIC states with algebraic [22] or compact [23] localization have been observed using photonic lattices. Also, very recently, BIC states driven by ac fields have been studied by Floquet theory [14] and the concept of Floquet BIC states has been introduced [25], i.e., BIC states that arise in a time-periodic Hamiltonian. In particular, the appearance of Floquet BIC states for a single particle hopping on a defective lattice, induced by a strong oscillating force, has been theoretically predicted. Nevertheless, such states suffer from the same drawback as BIC states of stationary

Hamiltonians, i.e., they are fragile and decay into resonances when the system parameters are slightly perturbed.

As happened in other contexts, moving to the many-particle framework makes the physics rather different. In a few recent works, it has been shown that particle interaction enhances the formation of BIC states and makes them robust [26–28]. Two-particle BIC states have been predicted to exist in *defective* Hubbard lattices, either in the bulk [26,27] or at the surface [28], but not in defect-free lattices. Such previous studies have been limited to consider *static* (i.e., undriven) Hubbard lattices. On the other hand, application of strong oscillating fields is known to strongly modify the dynamical and spectral properties of Hubbard systems. Strong fields can induce a dressing of the single- and many-particle states of the static system and eventually give rise to new phenomena, including the field-controlled superfluid-to-Mott-insulator phase transition [29], dynamic unbinding transitions in a periodically driven fermionic Mott-insulator at half filling [30], switching of particle interaction from repulsive to attractive [31], control of correlated tunneling and superexchange spin interactions [32], field-induced ferromagnetism [33], coherent destruction of correlation [34], and super Bloch oscillations [35].

In this paper, we introduce a type of robust two-particle bound state embedded in the continuum (BIC), which we call Floquet-Hubbard bound state in the continuum (FH BIC). Such states are induced in a *defect-free* Hubbard semilattice by application of an intense oscillating electric field. As opposed to single-particle Floquet BIC states [25], two-particle FH BIC modes are found in a wide range of parameter space and do not require fulfillment of resonance conditions, i.e., they are robust against perturbations of system parameters. A FH BIC mode basically corresponds to a molecular state in which the two particles bind together, undergoing correlated tunneling on the lattice [36–39]. Localization of the molecular state is induced by the external oscillating field, which effectively attracts the molecular state at the edge of the semi-infinite lattice. Analytical results, which explain the physical mechanism underlying the formation of FH BIC modes, are derived in the high-frequency limit of field modulation by a

*Corresponding author: giuseppe.dellavalle@polimi.it

multiple-time-scale asymptotic analysis of the ac-driven Hubbard Hamiltonian.

The paper is organized as follows. In Sec. II, we present Floquet numerical analysis of the two-particle ac-driven Hubbard Hamiltonian on a semilattice, and show the existence of FH BIC modes for a bichromatic driving field. In Sec. III, we consider the high-frequency regime of driving and develop multiple-time-scale asymptotic analysis to provide physical insights into the mechanism underlying the formation of the BIC states. In Sec. IV, we introduce a Bethe ansatz for the FH BIC states in the high-frequency modulation regime and determine analytically the domain of their existence in parameter space. Finally, the main conclusions are outlined in Sec. V.

II. PERIODICALLY DRIVEN TWO-PARTICLE FERMION-HUBBARD MODEL ON A SEMILATTICE: FLOQUET ANALYSIS

We consider two electrons with opposite spin hopping on a one-dimensional homogeneous semilattice with nearest-neighbor tunneling rate κ , driven by an intense oscillating electric field $E(t)$ [Fig. 1(a)]. The system is described by the driven Fermi-Hubbard (FH) Hamiltonian (see, e.g., Ref. [40] and references therein):

$$\hat{H} = \hat{H}_{\text{hop}} + \hat{H}_{\text{int}} + \hat{H}_{\text{drive}}, \quad (1)$$

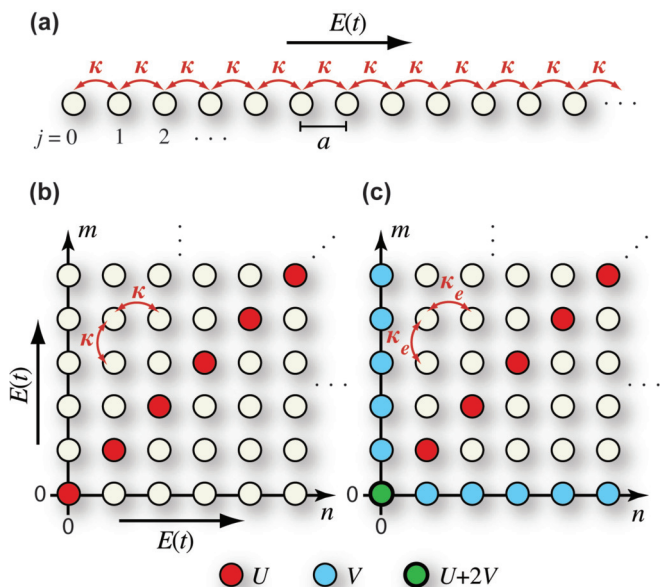


FIG. 1. (Color online) (a) Sketch of the one-dimensional tight-binding semilattice with applied ac electric field. The lattice is homogeneous (i.e., defect free). (b) Fock-space representation of the driven Hubbard Hamiltonian in the two-particle sector. The motion of the two electrons with opposite spins on the one-dimensional lattice in (a) is equivalent to the hopping dynamics of a single particle on a two-dimensional driven semi-infinite square lattice. (c) Effective static semilattice in the high-frequency limit retrieved by multiple-time-scale asymptotic analysis.

where

$$\hat{H}_{\text{hop}} = -\hbar\kappa \sum_{j=0}^{\infty} \sum_{\sigma=\uparrow,\downarrow} (\hat{a}_{j+1,\sigma}^\dagger \hat{a}_{j,\sigma} + \hat{a}_{j,\sigma}^\dagger \hat{a}_{j+1,\sigma}), \quad (2)$$

$$\hat{H}_{\text{int}} = U \sum_{j=0}^{\infty} \hat{n}_{j,\uparrow} \hat{n}_{j,\downarrow}, \quad (3)$$

$$\hat{H}_{\text{drive}} = -eaE(t) \sum_{j=0}^{\infty} j(\hat{n}_{j,\uparrow} + \hat{n}_{j,\downarrow}). \quad (4)$$

In previous equations, e is the elementary charge, a is the lattice constant, $U > 0$ is the on-site Coulomb repulsion energy of the two electrons, $\hat{a}_{j,\sigma}^\dagger$ and $\hat{a}_{j,\sigma}$ are the creation and annihilation operators, respectively, of a spin up ($\sigma = \uparrow$) or spin down ($\sigma = \downarrow$) electron at lattice sites $j = 0, 1, 2, \dots$, and $\hat{n}_{j,\sigma} = \hat{a}_{j,\sigma}^\dagger \hat{a}_{j,\sigma}$ is the particle-number operator at lattice site j for the σ spin electron. The external electric field can be written as $E(t) = E_0 f(t)$, where $f(t)$ is a dimensionless function with period $T = 2\pi/\omega$ and E_0 is the oscillation amplitude. In the case of noninteracting particles, i.e., for $U = 0$, the problem reduces to the single-particle case, which was previously studied by Garanovich and collaborators in Ref. [41]. Here the external oscillating field can induce surface bound states in the defect-free semilattice [41,42]. Such states, however, are not BIC states, rather they are ordinary normalizable states with a quasienergy outside the quasienergy spectrum of scattered states. The experimental observation of field-induced single-particle surface states of this kind was reported in Ref. [43]. As we will show in our work, the interplay of particle interaction and driving field enables one to observe bound states with a quasienergy embedded into the spectrum of scattered states, which we call Floquet-Hubbard BIC states (FH BIC). To this aim, let us indicate by $c_{n,m}(t)$ the amplitude probability to find the spin-up electron at lattice site n and the spin-down electron at lattice site m , i.e., let us expand the state vector $|\psi(t)\rangle$ of the system in Fock space as

$$|\psi(t)\rangle = \sum_{n,m=0}^{\infty} c_{n,m}(t) \hat{a}_{n,\uparrow}^\dagger \hat{a}_{m,\downarrow}^\dagger |0\rangle, \quad (5)$$

with $|0\rangle$ being the vacuum state. The evolution equations of the amplitude probabilities $c_{n,m}(t)$, as obtained after substitution of the decomposition (5) into the Schrödinger equation $i\hbar\partial_t|\psi\rangle = \hat{H}|\psi\rangle$, read

$$i\hbar \frac{dc_{n,m}}{dt} = -\hbar\kappa(c_{n-1,m} + c_{n+1,m} + c_{n,m-1} + c_{n,m+1}) + [U\delta_{n,m} - (n+m)eaE_0f(t)]c_{n,m}, \quad (6)$$

($n, m = 0, 1, 2, 3, \dots$), with $c_{-1,m} = c_{n,-1} = 0$.

Note that the above equations are equivalent to those governing the dynamics of a single electron hopping on a two-dimensional semilattice with diagonal site energy detuning and superposed ac driving field, as sketched in Fig. 1(b). Also, note that due to the symmetry of the Hamiltonian of Eqs. (1)–(4) with respect to particle exchange, the solutions to Eq. (6) can be classified as even, if $c_{m,n} = c_{n,m}$, or odd, if $c_{m,n} = -c_{n,m}$, with respect to particle exchange. Even solutions describe spin

singlets, whereas odd solutions span the sector of spin triplets (see, e.g., Ref. [40]).

To capture the effect of the oscillating external field, let us introduce the scaled time $\tau = \omega t$ and the gauge transformation $c_{n,m}(\tau) = b_{n,m}(\tau) \exp[i\Phi(\tau)(n+m)]$, where

$$\Phi(\tau) = \Gamma \int_0^\tau d\tau' f(\tau'/\omega), \quad (7)$$

and $\Gamma = (eaE_0)/(\hbar\omega)$ is the normalized forcing strength. The amplitude probabilities $b_{n,m}(\tau)$ then satisfy the following coupled equations:

$$i \frac{b_{n,m}}{d\tau} = -\frac{\kappa}{\omega} e^{-i\Phi(\tau)} [b_{n-1,m} + b_{n,m-1}] - \frac{\kappa}{\omega} e^{i\Phi(\tau)} [b_{n+1,m} + b_{n,m+1}] + \frac{U}{\hbar\omega} \delta_{n,m} b_{n,m}, \quad (8)$$

with $b_{-1,m} = b_{n,-1} = 0$.

The quasienergy spectrum of the driven Hubbard semilattice can be numerically computed by standard Floquet analysis of Eqs. (8). To this aim, we consider a finite lattice of N sites (with possibly N a large number), and map the $N \times N$ matrix of $b_{n,m}$ coefficients into a $M = N^2$ -dimensional column vector $\mathbf{B} = \{B_p\} = (B_0, B_1, B_2, \dots, B_{M-1})^T$ according to the rule $p = Nn + m$. By doing so, the system of Eqs. (8) is mapped into an equivalent ordinary differential equation system whose general solution can be written in the following form, according to Floquet theorem (see, e.g., Ref. [44]):

$$\mathbf{B}(\tau) = \mathcal{P}(\tau) e^{-i\mathcal{R}\tau} \mathbf{B}(0), \quad (9)$$

where $\mathbf{B}(0)$ is the initial value vector at time $\tau = 0$, $\mathcal{P}(\tau)$ is a $M \times M$ time-periodic matrix of period 2π with $\mathcal{P}(0)$ the identity matrix of rank M , and \mathcal{R} is a $M \times M$ time-independent matrix whose eigenvalues are the quasienergies (Floquet exponents) of the system [44]. The quasienergies can thus be computed from the eigenvalues η of the monodromy matrix $\mathcal{Q} = e^{-i\mathcal{R}2\pi}$ connecting the solution over one oscillation cycle (i.e., from $\tau = 0$ to $\tau = 2\pi$) according to the rule

$$\mathcal{E} = -\frac{\hbar\omega}{2\pi} \text{Im}\{\ln(\eta)\}, \quad (10)$$

where the $\hbar\omega$ factor is introduced to reframe the dynamics in the original time coordinate t . As is well known, quasienergies are defined apart from integer multiples of $\hbar\omega$, and conventionally they are restricted to the interval $-(\hbar\omega/2, \hbar\omega/2)$. To determine the monodromy matrix, note that the q th column of \mathcal{Q} can be retrieved as the numerical solution to Eqs. (8) under initial condition $B_p(0) = \delta_{p,q}$ with $p = 0, 1, 2, \dots, M-1$.

Once the quasienergies and corresponding quasienergy eigenvectors are determined, the search of bound states, either embedded (i.e., a BIC) or outside the spectrum of scattered states, is done by inspection of the participation ratio R of the N^2 quasienergy eigenvectors. The participation ratio of a quasienergy eigenmode $b_{n,m}(t)$ is defined as

$$R = \left[\sum_{n,m=0}^{N-1} |b_{n,m}|^2 \right]^2 / \sum_{n,m=0}^{N-1} |b_{n,m}|^4, \quad (11)$$

and turns out to be a periodic function of time with period $2\pi/\omega$. Usually one can limit to consider the value of R at a

given instant of the oscillation cycle, for example, at $t = 0$. For strongly localized (bound) states, $R \sim 1$, and for extended (scattered) states, $R \sim N^2$, whereas for extended molecular (doublonic) states [i.e., extended states but localized along the diagonal $n = m$ in the lattice of Fig. 1(b)], $R \sim N$. Hence, for N large enough, one can easily detect the existence of bound states, with quasienergy either embedded or outside the quasienergy band of scattered states. In our numerical simulations, we typically assumed $N = 41$ lattice sites.

We typically considered the weak-interaction regime $U < \sim \hbar\kappa$ and scanned a broad range of frequencies and amplitudes of the electric field, assuming either a monochromatic or a bichromatic wave form. With a monochromatic field $E(t) = E_0 \cos(\omega t)$, we could not observe BIC quasienergy eigenstates. Conversely, FH BIC states are found in the case of a bichromatic field $E(t) = E_0[\cos(\omega t) + \cos(2\omega t + \varphi)]$ for a wide range of values of normalized hopping rate $\epsilon = \kappa/\omega$, normalized forcing amplitude Γ , phase shift φ , and for a particle interaction energy $U = \epsilon^2 u \hbar\omega$, with $0 \leq u \leq 1$. Examples of FH BIC states at a low ($\epsilon = 0.9$), moderate ($\epsilon = 0.45$), and high ($\epsilon = 0.1$) modulation frequency are shown in Fig. 2 for $\varphi = 0$. An important property of the FH BIC states is that they are doublonic in nature, i.e., they emerge from the Hubbard band of molecular states, and are localized at one edge of the semilattice. This explains the physical origin of FH BIC modes: particle interaction binds together the two particles, which cannot dissociate because of quasienergy conservation and thus undergo correlated tunneling [36,37]; the external field then pushes the bound molecular state near the edge of the lattice. The mechanism underlying field-induced surface localization of the molecular state will be clarified in the next section. In our numerical analysis, the doublonic nature of the FH BIC states was ascertained by inspecting, in Fock space, the quasienergy eigenstate with minimal participation ratio (marked with red circles in the quasienergy spectra of Fig. 2 and highlighted by arrows), as detailed in the lower panels of Fig. 2. Note that in all three cases [Figs. 2(a)–2(c)], the FH BIC state entails excitation of the diagonal elements with negligible contribution from the neighboring diagonals. This corresponds to both electrons occupying the same lattice site, i.e., it is a Hubbard state, with negligible excitation of single-particle states (corresponding to nondiagonal elements in the lower panels of Fig. 2). Note also that the FH BIC state is localized at the corner $n = 0, m = 0$ of the Fock lattice of Fig. 1(b), so that it corresponds to a two-particle surface state of the Tamm type in the original one-dimensional lattice. The localization of the FH BIC increased under high-frequency driving as compared to the low-frequency driving. Finally, we found that if particle interaction is neglected, no BIC states are observed for the driving conditions considered in our simulations, even in the high-frequency regime, as shown in Fig. 2(d). In this case, the state with minimum participation ratio [which is, in any case, an order of magnitude larger as compared to the participation ratio of the doublonic BIC in this same driving regime, shown in Fig. 2(c)] entails excitation of the antidiagonal elements only, with complete delocalization along the antidiagonal. This state turns out to have zero energy and π phase shift between the $b_{n,m}$ coefficients of neighboring Fock basis elements. As discussed in Sec. IV B, the appearance of this state is caused by truncation of the semilattice and has

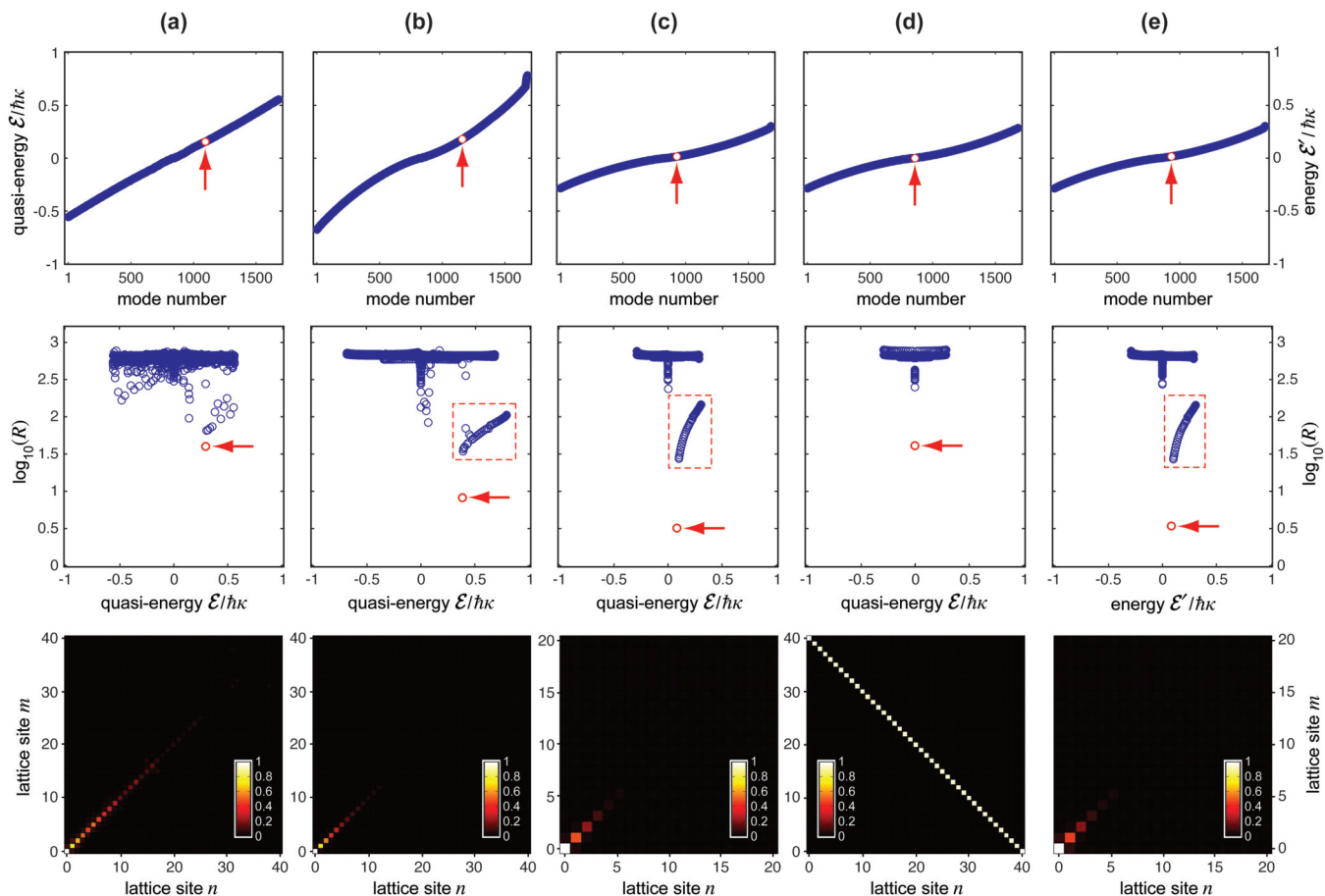


FIG. 2. (Color online) Quasienergy spectrum (top panels), participation ratio spectrum (middle panels), and BIC quasienergy eigenstate $|b_{n,m}(0)\rangle^2$ (bottom panels) for the two-particle semilattice driven under different regimes: (a) low frequency $\kappa/\omega = 0.9$, $\Gamma = 4.5$, $u = 0.5$; (b) moderate frequency $\kappa/\omega = 0.5$, $\Gamma = 4.2$, $u = 1$; and (c) high frequency $\kappa/\omega = 0.1$, $\Gamma = 3.0$, $u = 1$. (d) Same as (c) but for noninteracting particles ($u = 0$). (e) Energy spectrum, participation ratio spectrum, and BIC eigenstate of the effective static lattice corresponding to the high-frequency driving regime shown in (c). In the bottom panels, the amplitude coefficients are normalized to the peak value for clarity. Arrows indicate the state with minimum participation ratio. The red box comprises the scattered doublonic states (belonging to the Mott-Hubbard band).

no special physical meaning in a true (i.e., infinite) semilattice. Finally, it should be noted that, as opposed to single-particle Floquet BIC states recently predicted in Ref. [25], two-particle FH BIC states are robust. In fact, single-particle Floquet BIC states exist solely at very special values of normalized forcing Γ , and are thus fragile states because even a small change of the driving amplitude transforms the BIC (normalizable) mode into a resonance (non-normalizable) state. Conversely, FH BIC modes in the driven Hubbard model do not require exact tuning of the external parameters, are robust against parameter change or fluctuations, and are even thresholdless, as discussed in the next sections.

III. MULTIPLE-TIME-SCALE ASYMPTOTIC ANALYSIS

To get deeper physical insights into the properties and the mechanism underlying the formation of FH BIC states, we performed a multiple-time-scale asymptotic analysis (MT-SAA) of the driven two-particle Hubbard lattice in the high-frequency limit $\omega \gg \kappa$ (see, for instance, [45,46]). To this aim, let us look for a solution to Eqs. (8) as a power-series expansion

in the smallness parameter $\epsilon = \kappa/\omega$:

$$b_{n,m}(\tau) = b_{n,m}^{(0)}(\tau) + \epsilon b_{n,m}^{(1)}(\tau) + \epsilon^2 b_{n,m}^{(2)}(\tau) + \dots \quad (12)$$

To remove the appearance of secularly growing terms in the asymptotic analysis that would prevent the validity of above expansion, let us introduce the multiple time scales,

$$\tau_0 = \tau, \quad \tau_1 = \epsilon\tau, \quad \tau_2 = \epsilon^2\tau, \quad \dots \quad (13)$$

This gives rise to the derivative rule $d/d\tau = \partial_{\tau_0} + \epsilon\partial_{\tau_1} + \epsilon^2\partial_{\tau_2} + \dots$. Substitution of the ansatz (12) into Eqs. (8) and collection of the terms of the same order in ϵ allows one to derive a hierarchy of equations for successive corrections to $b_{n,m}$ at various orders. At leading order ($\sim\epsilon^0$), one simply obtains $\partial_{\tau_0} b_{n,m}^{(0)} = 0$, which yields

$$b_{n,m}^{(0)} = C_{n,m}(\tau_1, \tau_2, \dots), \quad (14)$$

where the amplitudes $C_{n,m}$ vary on the slower time scales τ_1, τ_2, \dots . The equations at higher orders ($\sim\epsilon^k, k \geq 1$) have the general form

$$i\partial_{\tau_0} b_{n,m}^{(k)} = -i\partial_{\tau_k} C_{n,m} + G_{n,m}^{(k)}(\tau_0; b_{n,m}^{(j < k)}), \quad (15)$$

where $G_{n,m}^{(k)}$ depends explicitly on τ_0 and on the solutions $b_{n,m}^{(j)}$ at previous orders $j = 0, 1, \dots, k-1$. To avoid the occurrence of secular growing terms in the solution $b_{n,m}^{(k)}$, the following solvability condition must be satisfied:

$$i \partial_{\tau_k} C_{n,m} = \langle G_{n,m}^{(k)} \rangle, \quad (16)$$

where $\langle \cdot \rangle$ denote the dc component of the driving term $G_{n,m}^{(k)}$. Equation (16) determines the evolution of the amplitude $C_{n,m}$ on the slow time scale τ_k ; the correction at order k can be then calculated as

$$b_{n,m}^{(k)} = -i \int_0^{\tau_0} d\xi (G_{n,m}^{(k)} - \langle G_{n,m}^{(k)} \rangle). \quad (17)$$

In particular, at order $\sim \epsilon$, one has

$$G_{n,m}^{(1)} = -(C_{n-1,m} + C_{n,m-1})e^{-i\Phi(\tau_0)} - (C_{n+1,m} + C_{n,m+1})e^{i\Phi(\tau_0)}, \quad (18)$$

with $C_{-1,m} = C_{n,-1} = 0$. To further proceed in the analysis, it is worth introducing the Fourier expansion of the phase term $\exp[-i\Phi(\tau_0)]$ by letting

$$\exp[-i\Phi(\tau_0)] = \Theta_0 + \sum_{l \neq 0} \Theta_l \exp(il\tau_0), \quad (19)$$

where Θ_l are the Fourier coefficients.

Note that at the present order of approximation, the oscillating terms in Eq. (19) are averaged out in the solvability condition of Eq. (16) (with $k=1$). This is the so-called rotating-wave approximation. Therefore, the evolution of amplitude probabilities up to the time scale $\sim 1/(\omega\epsilon)$ is given by $i(dC_{n,m}/dt) = i\omega(\partial_{\tau_0} + \epsilon\partial_{\tau_1})C_{n,m} = i\epsilon\partial_{\tau_1}C_{n,m}$, and reads

$$i \frac{dC_{n,m}}{dt} = -\Theta_0 \kappa (C_{n-1,m} + C_{n,m-1}) - \Theta_0^* \kappa (C_{n+1,m} + C_{n,m+1}), \quad (20)$$

with $C_{-1,m} = C_{n,-1} = 0$. The latter equation system represents a homogeneous (defect-free) static semilattice with renormalized tunneling rate $\Theta_0 \kappa$. As is well known, this lattice cannot sustain bound states, but rather scattered states only. Therefore, multiple-scale asymptotic analysis ought to be pushed beyond the rotating-wave approximation. To do this, we have to consider Θ_0 to be of the order of ϵ , meaning that the driving field operates close to the coherent-destruction of tunneling (CDT) condition [45] (see also the review paper of Ref. [47]), so that higher-order processes can compete with the renormalized tunneling at previous order. The evolution equations of the amplitudes $C_{n,m}$ on the slow time scale τ_2 can then be obtained after some lengthy but straightforward calculations following the procedure outlined above, once the corrections to $b_{n,m}$ at order $\sim \epsilon$ are calculated using Eq. (17) and the solvability condition at order $\sim \epsilon^2$ [Eq. (16)] is explicitly written down. If we stop the asymptotic analysis at the order ϵ^2 , the temporal evolution of the amplitude probabilities $C_{n,m}(t)$, valid up to the long time scale $\sim 1/(\omega\epsilon^2)$, now becomes

$$i \hbar \frac{dC_{n,m}}{dt} = -\hbar \kappa_e (C_{n-1,m} + C_{n+1,m} + C_{n,m-1} + C_{n,m+1}) + V[\delta_{n,0} + \delta_{m,0}]C_{n,m} + U \delta_{n,m} C_{n,m}, \quad (21)$$

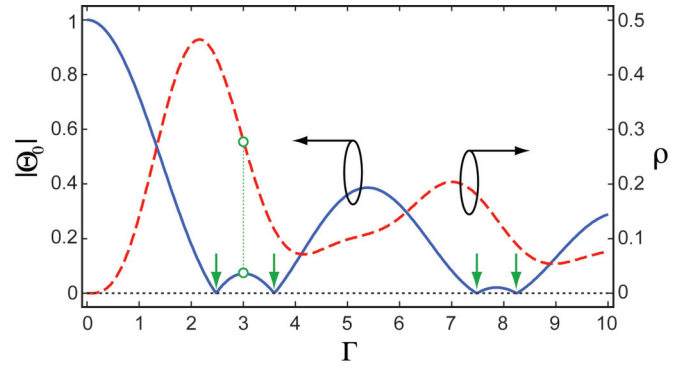


FIG. 3. (Color online) Behavior of $|\Theta_0|$ and ρ as a function of the normalized field amplitude Γ . Vertical arrows point out the first four values of Γ for which CDT is achieved. Red dots refer to the driving conditions employed in the simulations of Fig. 2(c).

with $C_{-1,m} = C_{n,-1} = 0$. In Eqs. (21), we have set (without loss of generality [48]) $\kappa_e = |\Theta_0| \kappa$, and V is an effective boundary potential induced by the external field, whose expression reads

$$V \equiv - \left(\frac{\kappa}{\omega} \sum_{l \neq 0} \frac{|\Theta_l|^2}{l} \right) \hbar \kappa \equiv -\rho \frac{\hbar \kappa^2}{\omega}, \quad (22)$$

where $\rho \equiv \sum_{l \neq 0} |\Theta_l|^2 / l$. Equations (21) and (22) are the main result of the multiple-scale analysis at order $\sim \epsilon^2$, and show that the original defect-free driven semilattice of Fig. 1(b), in the high-frequency regime and close to the CDT condition, is equivalent to a static semilattice with renormalized tunneling rate and boundary defects induced by the time-periodic driving; see Fig. 1(c). Such field-induced edge defects in the equivalent lattice model justify the appearance of surface Tamm states of the Floquet type. An inspection of Eq. (22) shows that this possibility is prevented under monochromatic driving. Actually, in this case, the Fourier coefficients in the expansion of Eq. (19) satisfy the condition $|\Theta_{-l}| = |\Theta_l|$ for any $l \neq 0$, resulting in $V = 0$ according to Eq. (22). Hence, for a monochromatic driving field, the main effect is renormalization of the hopping rate; however, localization of bound molecular states is prevented [49]. This is not the case for a bichromatic field for which, in general, $|\Theta_{-l}| \neq |\Theta_l|$. As an example, in Fig. 3 we plot the behavior of $|\Theta_0|$ and ρ versus the normalized forcing amplitude $\Gamma = eaE_0/(\hbar\omega)$ for a bichromatic field $E(t) = E_0 \cos(\omega t) + E_0 \cos(2\omega t + \varphi)$ with $\varphi = 0$. Note that the CDT condition is attained at $\Gamma = \Gamma_0 \simeq 2.4787, 3.593, 7.485, 8.242, \dots$, and that for a driving amplitude Γ near Γ_0 , the parameter ρ (and hence the defect energy V) is nonvanishing.

To give a reason for the doublonic and BIC nature of the Floquet BIC states found in the numerical simulations under high-frequency bichromatic driving, we computed the energy spectrum and participation ratio of the eigenstates for the effective static lattice detailed by Eqs. (21) and (22) [50]. Results corresponding to the case of high-frequency driving reported in Fig. 2(c) are shown in Fig. 2(e). The two spectra [top panels in Figs. 2(c) and 2(e)] are in excellent quantitative agreement, both for the single-particle states and for the doublonic states of the Mott-Hubbard band (comprised in the rectangular box

in Fig. 2). Most importantly, the effective static lattice predicts exactly the same doublonic BIC state as the one observed in the original driven lattice: energy $\mathcal{E}'/(\hbar\kappa) = 8.16 \times 10^{-2}$ and participation ratio $R = 3.42$, against quasienergy $\mathcal{E}/(\hbar\kappa) = 8.13 \times 10^{-2}$ and participation ratio $R = 3.22$. We performed several simulations with different values of parameters and found that in the high-frequency limit (i.e., $\epsilon < 0.1$) and close to CDT, the MT-SAA matches the Floquet numerical results on the BIC state with an error $e = (\mathcal{E}' - \mathcal{E})/\mathcal{E}'$, which is small, of the order of ϵ^2 .

IV. PROPERTIES OF THE FLOQUET-HUBBARD BIC STATE IN THE HIGH-FREQUENCY LIMIT

A. Existence conditions and intrinsic robustness

Since the solutions for the energy spectrum and corresponding eigenstates of Eqs. (21) can be derived analytically, it is possible to retrieve the exact conditions for the existence of the FH BIC, at least in the regime where MT-SAA is accurate. To do so, note that according to the Bethe ansatz [40], any eigensolution to Eqs. (21) can be written as (see also [26,28])

$$C_{n,m} = (A_1 z_1^n z_2^m + A_2 z_1^{-n} z_2^m + A_3 z_1^n z_2^{-m} + A_4 z_1^{-n} z_2^{-m} + A_5 z_2^n z_1^m + A_6 z_2^{-n} z_1^m + A_7 z_2^n z_1^{-m} + A_8 z_2^{-n} z_1^{-m}) \times \exp[-i(\mathcal{E}'/\hbar)t], \quad (23)$$

for $n \geq m$, and $C_{m,n} = \pm C_{n,m}$. In Eq. (23), A_1, A_2, \dots, A_8 are eight complex amplitudes to be determined, $z_{1,2} = \exp(ik_{1,2})$, and k_1, k_2 are two complex wave numbers that define the energy of the eigenstate according to the relation

$$\mathcal{E}' = -\hbar\kappa_e(z_1 + z_1^{-1} + z_2 + z_2^{-1}). \quad (24)$$

A solvability condition is obtained by imposing the validity of Eq. (23) and Eqs. (21) along the two defective lines corresponding to $m = n$ and $n = 0$ (or, equivalently, $m = 0$). This way, a set of eight homogeneous linear equations for the amplitudes A_l is retrieved, namely, $\mathcal{T}\mathbf{v} = 0$, where $\mathbf{v} = (A_1, A_2, \dots, A_8)^T$ and \mathcal{T} is a 8×8 matrix. Note that Hubbard states having nonzero value of some diagonal elements ($C_{n,n}$) ought to be even with respect to particle exchange, meaning that the FH BIC state we are seeking can only exist for spin-singlet Floquet states and not for spin triplets. If we consider even states only, the nonzero elements of \mathcal{T} turn out to be given by

$$\begin{aligned} \mathcal{T}_{11} &= \mathcal{T}_{48} = z_1 + 1/z_2 + (\mathcal{E}' - U)/(2\hbar\kappa_e), \\ \mathcal{T}_{15} &= \mathcal{T}_{44} = z_2 + 1/z_1 + (\mathcal{E}' - U)/(2\hbar\kappa_e), \\ \mathcal{T}_{22} &= \mathcal{T}_{36} = 1/z_1 + 1/z_2 + (\mathcal{E}' - U)/(2\hbar\kappa_e), \\ \mathcal{T}_{27} &= \mathcal{T}_{33} = z_1 + z_2 + (\mathcal{E}' - U)/(2\hbar\kappa_e), \\ \mathcal{T}_{51} &= \mathcal{T}_{62} = 1/z_2 + V/(\hbar\kappa_e), \\ \mathcal{T}_{53} &= \mathcal{T}_{64} = z_2 + V/(\hbar\kappa_e), \\ \mathcal{T}_{75} &= \mathcal{T}_{86} = 1/z_1 + V/(\hbar\kappa_e), \\ \mathcal{T}_{77} &= \mathcal{T}_{88} = z_1 + V/(\hbar\kappa_e). \end{aligned} \quad (25)$$

The homogeneous linear system $\mathcal{T}\mathbf{v} = 0$ admits a solution for any k_1 and k_2 because $\det(\mathcal{T}) = 0$. Therefore, k_1 and k_2 are constrained only by the condition that $C_{n,m}$ does not

diverge as $n, m \rightarrow \infty$ (leading to a real energy spectrum \mathcal{E}'). In particular, any FH doublonic bound state, with spectrum either inside (a BIC) or not inside the band of scattered states, ought to be represented by the solution with $A_l = 0$ for $l \neq 1$, $\text{Im}\{k_1\} > 0$, $\text{Im}\{k_1 + k_2\} > 0$, for $n \geq m$, and $C_{m,n} = \pm C_{n,m}$ for symmetry reasons. The conditions on $k_{1,2}$ guarantee the correct exponential decay towards zero as $n, m \rightarrow \infty$ for a doublonic state. Being A_1 is the only nonzero amplitude in the Bethe ansatz, the solvability condition $\mathcal{T}\mathbf{v} = 0$ simplifies to $\mathcal{T}_{11} = \mathcal{T}_{51} = 0$, which, combined with Eq. (24), allows one to determine the expressions for $z_{1,2}$ as a function of the U , V , and κ_e parameters:

$$\begin{aligned} \frac{1}{z_1} &= \frac{1}{2} \left(\frac{\hbar\kappa_e}{V} - \frac{V+U}{\hbar\kappa_e} \right) \pm \sqrt{\frac{1}{4} \left(\frac{\hbar\kappa_e}{V} - \frac{V+U}{\hbar\kappa_e} \right)^2 + 1}, \\ \frac{1}{z_2} &= -\frac{V}{\hbar\kappa_e}. \end{aligned} \quad (26)$$

From Eq. (26), the complex wave numbers of the FH state are then retrieved as $k_{1,2} = i \ln(1/z_{1,2})$. By imposing $\text{Im}\{k_1\} > 0$ and $\text{Im}\{k_1 + k_2\} > 0$, it is found that a FH doublonic bound state always exists for $UV < 0$, whereas for $UV > 0$, it is forbidden only if $|U|/\hbar\kappa_e < 2(\hbar\kappa_e/|V| - |V|/\hbar\kappa_e)$. To be a BIC state, its energy \mathcal{E}' ought to be embedded in the interval $(-4\hbar\kappa_e, 4\hbar\kappa_e)$ of the two-particle scattered eigenstates, and this results in the following conditions for our case of repulsing particles ($U > 0$):

$$\begin{aligned} f_1(U) &< V/(\hbar\kappa_e) < 0 \quad \text{for } U < 4\hbar\kappa_e, \\ f_1(U) &< V/(\hbar\kappa_e) < f_2(U) \quad \text{for } U \geq 4\hbar\kappa_e, \end{aligned} \quad (27)$$

where

$$\begin{aligned} f_1(U) &= -\frac{U}{2\hbar\kappa_e} - \sqrt{\left(\frac{U}{2\hbar\kappa_e}\right)^2 + 1}, \\ f_2(U) &= 8 - \frac{1}{2} \left(\frac{U}{\hbar\kappa_e}\right)^2 - \frac{U}{2\hbar\kappa_e} \sqrt{\left(\frac{U}{\hbar\kappa_e}\right)^2 - 16}. \end{aligned} \quad (28)$$

The inequalities given in Eqs. (27) and (28) define the domain of existence of the FH BIC state in the high-frequency regime and close to the CDT, which is shown in Fig. 4. Note that the FH BIC state is thresholdless with respect to the induced lattice defect V , provided that the interaction energy $U < 4\hbar\kappa_e$ (which is in line with our hypothesis of weakly interacting electrons). Indeed, in our simulations, we assumed $U = u\epsilon^2\hbar\omega = u\epsilon\hbar\kappa = (u\epsilon/|\Theta_0|)\hbar\kappa_e$ and for the driving parameters considered in the case of Figs. 2(c)–2(e), i.e., $\epsilon = 0.1$, $|\Theta_0| = 7.18 \times 10^{-2}$, $u = 1$, we have $U \simeq 1.39\hbar\kappa_e$, i.e., in accord with the thresholdless regime (cf. Fig. 4).

We conclude that in the high-frequency regime and close to CDT, a FH BIC state always exists in a system of two weakly interacting electrons hopping on a one-dimensional semilattice driven by a bichromatic electric field. Note that this is a completely distinctive feature of the many-body system as compared to the single-particle system, since it is well known that a single-particle Tamm state requires for its existence an effective boundary defect potential V exceeding in absolute value the effective tunneling rate $\hbar\kappa_e$. Indeed, in the simulations of Figs. 2(c) and 2(d), the effective static potential

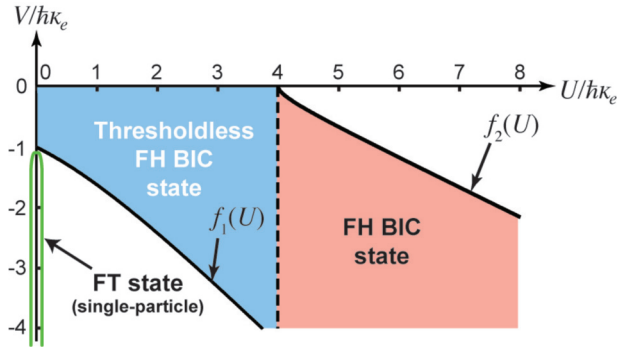


FIG. 4. (Color online) Domain of existence of the Floquet-Hubbard BIC state under high-frequency driving limit (shaded area). The FH BIC is thresholdless for $U < 4\hbar\kappa_e$. Domain of existence of the single-particle Floquet Tamm (FT) state is also shown (half line on the vertical axis).

$V = -2.79 \times 10^{-2} \hbar\kappa$, whereas $\hbar\kappa_e = |\Theta_0| \hbar k \simeq 7.18 \times 10^{-2} \hbar\kappa$, thus the formation of single-particle Tamm states is forbidden. Note also that Eqs. (27) and (28) forbid the coexistence of FH BIC states and single-particle Tamm states of the Floquet type [Fig. 4(a)].

Finally, it is worth mentioning that (for $U > 0$) the quasienergy of the FH BIC state is lower than the interaction energy U , regardless of the value of V and κ_e parameters, i.e., the FH BIC energy lies below the effective Mott-Hubbard band $[U, (U^2 + 16\hbar^2\kappa_e^2)^{1/2}]$ of scattered doublonic states [40]. This means that the FH BIC mode is thermodynamically favored among the Hubbard states of the driven semilattice.

B. Switching of the Floquet-Hubbard BIC localization in a finite lattice

In our simulations, we considered a finite lattice, i.e., a truncated semilattice. It is worth noting that truncation of the semilattice causes a modification of Eqs. (21), and the correct equivalent static lattice corresponding to the high-frequency limit of a truncated driven semilattice with N sites (indexed from 0 to $N - 1$) turns out to be the following:

$$i\hbar \frac{dC_{n,m}}{dt} = -\hbar\kappa_e [C_{n-1,m} + C_{n+1,m} + C_{n,m-1} + C_{n,m+1}] + V[\delta_{n,0} + \delta_{m,0} - \delta_{n,N-1} - \delta_{m,N-1}]C_{n,m} + U\delta_{n,m}C_{n,m}, \quad (29)$$

with $C_{-1,m} = C_{n,-1} = C_{N,m} = C_{n,N} = 0$. Indeed, as indicated in previous sections (see note [50]), we implemented Eqs. (29) and not Eqs. (21) in our simulations. Note that the truncation of the semilattice induces a defect at the $n = N - 1$ and $m = N - 1$ boundaries with opposite sign as compared to the defect induced at the $n = 0$ and $m = 0$ boundaries. Note also that for noninteracting particles ($U = 0$), the truncated semilattice becomes antisymmetric with respect to the antidiagonal of Fock space and this explains the origin of the state with minimum participation ratio observed in Fig. 2(d), having zero energy and complete delocalization along the antidiagonal with π phase difference between neighboring sites (cf. Sec. II). Actually, this state is represented by $C_{n,m} = \delta_{n,N-1-m}$ for even n and $C_{n,m} = -\delta_{n,N-1-m}$ for odd n . It is not difficult to verify,

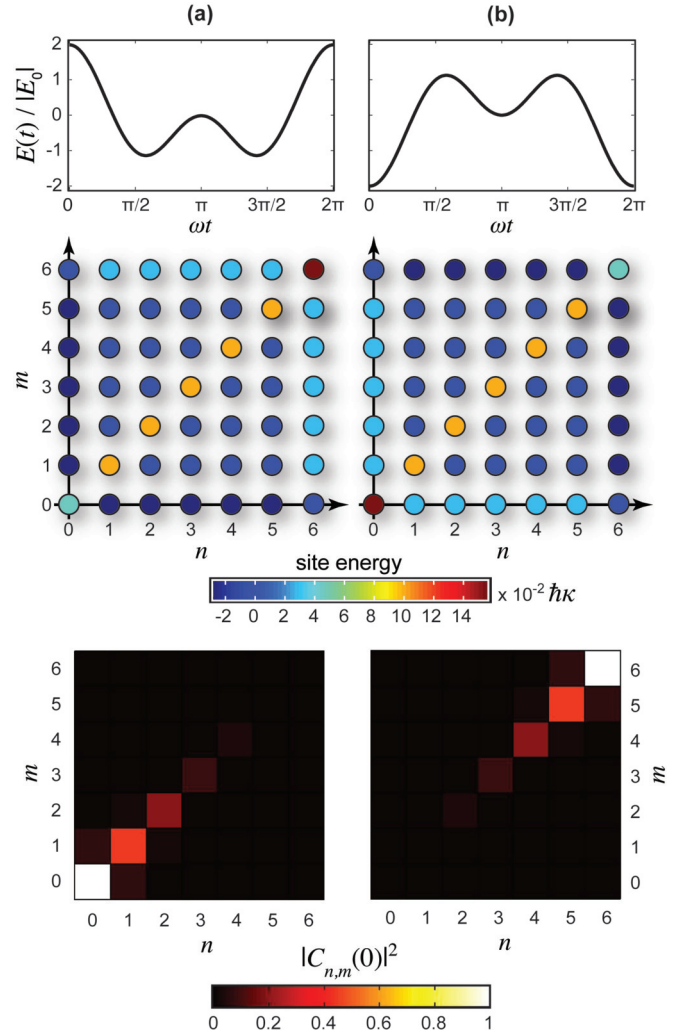


FIG. 5. (Color online) Switching of the FH BIC localization in a small ($N = 7$) finite lattice: driving field (top panels), lattice site energies (middle panels), and Fock-space representation of the FH BIC (bottom panels) for (a) positive field amplitude ($E_0 > 0$) and (b) negative field amplitude ($E_0 < 0$). Driving parameters and particle interaction are the same as in the simulations of Fig. 2(c).

by direct substitution into Eqs. (29) with $U = 0$, that this is an eigenstate of the lattice with zero energy.

Interestingly, we found that truncation effects can be exploited to achieve switching of FH BIC localization from one boundary to the other one. The concept is illustrated in Fig. 5 for a small lattice with $L = 7$ sites. Rather generally, for a given driving regime, the existence condition of the FH BIC state can be fulfilled at one lattice boundary (at the left edge for $V > 0$, at the right edge for $V < 0$), but not at the opposite one. In the simulations of previous sections, we considered a positive normalized field amplitude Γ , causing the negative defective potential to be induced at the $n = 0$, $m = 0$ boundaries [Fig. 5(a)]. The localization is reversed, i.e., exactly the same FH BIC state is localized at the opposite boundary $n = N - 1$, $m = N - 1$, by simply changing the sign of the electric-field amplitude E_0 (and thus of Γ), as shown in Fig. 5(b). This can be easily understood by noting that a sign change of Γ implies, according to Eq. (7), complex

conjugation of Eq. (19), resulting in a change of sign in the series of Eq. (22), and thus in V . Such a switching feature of the FH BIC localization is possible even though the driving field has zero mean value because for bichromatic driving a sign change of the amplitude E_0 does not correspond to a time shift by half a period (contrary to, e.g., the monochromatic case) [cf. top panels in Fig. 5].

V. CONCLUSION

In this work, we have numerically and analytically demonstrated a type of two-particle BIC state in ac-driven semi-infinite Hubbard lattices. As particle interaction is responsible for correlated tunneling and the formation of a molecular bound state (doublon) [36,37], the additional external field introduces an effective attractive potential that localizes the molecular state at the lattice edge. Noticeably, the quasienergy of the particle bound state localized at the lattice surface can be embedded into the quasienergy spectrum of scattered states, i.e., it realizes a Floquet BIC state. As compared to

single-particle Floquet BIC states [28], which are fragile states and whose existence requires fulfillment of certain resonance conditions, the Hubbard-Floquet BIC states are intrinsically robust and exhibit other peculiar features: they are the states with the lowest quasienergy among the molecular states of the driven Hubbard semilattice, and, in a finite lattice, their localization can be switched from one boundary to the other one by simply changing the direction of the bichromatic field. Finally, it is worth noticing that our results hold for two interacting bosons on a semilattice as well, since the FH BIC state is symmetric under particle exchange regardless of the statistics (fermionic or bosonic). Further investigations should explore the effect of a phase shift between the two components of the bichromatic driving, the existence of FH states outside the continuum, and the possibility to generalize the technique to higher-dimensional lattices. We believe that our results could pave the way for the development of BIC physics in the context of many-body theories, with application to driven quasi-one-dimensional correlated crystals [51,52] and quantum simulators of interacting-particles systems based on cold atoms [53] or photonic lattices [54].

-
- [1] J. von Neumann and E. Wigner, *Z. Phys.* **30**, 465 (1929).
 - [2] F. H. Stillinger and D. R. Herrick, *Phys. Rev. A* **11**, 446 (1975).
 - [3] F. Capasso, C. Sirtori, J. Faist, D. L. Sivco, S.-N. G. Chu, and A. Y. Cho, *Nature (London)* **358**, 565 (1992).
 - [4] H. Friedrich and D. Wintgen, *Phys. Rev. A* **31**, 3964 (1985).
 - [5] H. Friedrich and D. Wintgen, *Phys. Rev. A* **32**, 3231 (1985).
 - [6] U. Fano, *Phys. Rev.* **124**, 1866 (1961).
 - [7] J. Falst, F. Capasso, C. Sirtori, K. W. West, and L. N. Pfeiffer, *Nature (London)* **390**, 589 (1997).
 - [8] H. Schmidt, K. L. Campman, A. C. Gossard, and A. Imamoglu, *Appl. Phys. Lett.* **70**, 3455 (1997).
 - [9] H. Kataura, Y. Kumazawa, Y. Maniwa, I. Umezū, S. Suzuki, Y. Ohtsuka, and Y. Achiba, *Synth. Met.* **103**, 2555 (1999).
 - [10] B. R. Bulka and P. Stefanski, *Phys. Rev. Lett.* **86**, 5128 (2001).
 - [11] J. Gores, D. Goldhaber-Gordon, S. Heemeyer, M. A. Kastner, H. Shtrikman, D. Mahalu, and U. Meirav, *Phys. Rev. B* **62**, 2188 (2000).
 - [12] B. Luk'Yanchuk, N. I. Zheludev, S. A. Maier, N. J. Halas, P. Nordlander, H. Giessen, and C. T. Chong, *Nat. Mater.* **9**, 707 (2010).
 - [13] A. E. Miroshnichenko, S. Flach, and Y. S. Kivshar, *Rev. Mod. Phys.* **82**, 2257 (2010).
 - [14] C. Gonzalez-Santander, P. A. Orellana, and F. Dominguez-Adame, *Europhys. Lett.* **102**, 17012 (2013).
 - [15] J. P. Ramos and P. A. Orellana, [arXiv:1304.8059](https://arxiv.org/abs/1304.8059).
 - [16] L. Fonda and R. G. Newton, *Ann. Phys.* **10**, 490 (1960).
 - [17] Bohm-Jung Yang, Mohammad Saeed Bahramy, and Naoto Nagaosa, *Nat. Comm.* **4**, 1524 (2013).
 - [18] D. C. Marinica, A.G. Borisov, and S.V. Shabanov, *Phys. Rev. Lett.* **100**, 183902 (2008).
 - [19] Y. Plotnik, O. Peleg, F. Dreisow, M. Heinrich, S. Nolte, A. Szameit, and Mordechai Segev, *Phys. Rev. Lett.* **107**, 183901 (2011).
 - [20] M. I. Molina, A. E. Miroshnichenko, and Y. S. Kivshar, *Phys. Rev. Lett.* **108**, 070401 (2012).
 - [21] C. W. Hsu, B. Zhen, J. Lee, S.-L. Chua, S. G. Johnson, J. D. Joannopoulos, and M. Soljacic, *Nature (London)* **499**, 188 (2013).
 - [22] G. Corrielli, G. Della Valle, A. Crespi, R. Osellame, and S. Longhi, *Phys. Rev. Lett.* **111**, 220403 (2013).
 - [23] S. Weimann, Y. Xu, R. Keil, A. E. Miroshnichenko, S. Nolte, A. A. Sukhorukov, A. Szameit, and Y. S. Kivshar, *Phys. Rev. Lett.* **111**, 240403 (2013).
 - [24] Chang-Ling Zou, Jin-Ming Cui, Fang-Wen Sun, Xiao Xiong, Xu-Bo Zou, Zheng-Fu Han, and Guang-Can Guo, [arXiv:1305.5297v1](https://arxiv.org/abs/1305.5297v1).
 - [25] S. Longhi and G. Della Valle, *Sci. Rep.* **3**, 2219 (2013).
 - [26] J. M. Zhang, D. Braak, and M. Kollar, *Phys. Rev. Lett.* **109**, 116405 (2012).
 - [27] J. M. Zhang, D. Braak, and M. Kollar, *Phys. Rev. A* **87**, 023613 (2013).
 - [28] S. Longhi and G. Della Valle, *J. Phys.: Condens. Matter* **25**, 235601 (2013).
 - [29] A. Zenesini, H. Lignier, D. Ciampini, O. Morsch, and E. Arimondo, *Phys. Rev. Lett.* **102**, 100403 (2009).
 - [30] F. Hassler, A. Rügge, M. Sigrist, and G. Blatter, *Phys. Rev. Lett.* **104**, 220402 (2010).
 - [31] N. Tsuji, T. Oka, P. Werner, and H. Aoki, *Phys. Rev. Lett.* **106**, 236401 (2011).
 - [32] Y. A. Chen, S. Nascimbene, M. Aidelsburger, M. Atala, S. Trotzky, and I. Bloch, *Phys. Rev. Lett.* **107**, 210405 (2011).
 - [33] G. Della Valle and S. Longhi, *Europhys. Lett.* **101**, 67006 (2013).
 - [34] S. Longhi and G. Della Valle, *Phys. Rev. A* **86**, 042104 (2012).
 - [35] S. Longhi and G. Della Valle, *Phys. Rev. B* **86**, 075143 (2012).

- [36] K. Winkler, G. Thalhammer, F. Lang, R. Grimm, J. Hecker Denschlag, A. J. Daley, A. Kantian, H. P. Büchler, and P. Zoller, *Nature (London)* **441**, 853 (2006).
- [37] S. Fölling, S. Trotzky, P. Cheinet, M. Feld, R. Saers, A. Widera, T. Müller, and I. Bloch, *Nature (London)* **448**, 1029 (2007).
- [38] M. Valiente and D. Petrosyan, *J. Phys. B: At. Mol. Opt. Phys.* **41**, 161002 (2008).
- [39] N. Strohmaier, D. Greif, R. Jordens, L. Tarruell, H. Moritz, T. Esslinger, R. Sensarma, D. Pekker, E. Altman, and E. Demler, *Phys. Rev. Lett.* **104**, 080401 (2010).
- [40] F. H. L. Essler, H. Frahm, F. Göhmann, A. Klümper, and V. E. Korepin, *The One-Dimensional Hubbard Model* (Cambridge University Press, Cambridge, 2005).
- [41] I. L. Garanovich, A. A. Sukhorukov, and Y. S. Kivshar, *Phys. Rev. Lett.* **100**, 203904 (2008).
- [42] I. L. Garanovich, S. Longhi, A. A. Sukhorukov, and Y. S. Kivshar, *Phys. Rep.* **518**, 1 (2012).
- [43] A. Szameit, I. L. Garanovich, M. Heinrich, A. A. Sukhorukov, F. Dreisow, T. Pertsch, S. Nolte, A. Tunnermann, and Y. S. Kivshar, *Phys. Rev. Lett.* **101**, 203902 (2008).
- [44] G. Teschl, *Ordinary Differential Equations and Dynamical Systems* (American Mathematical Society, Providence, 2010).
- [45] S. Longhi, *Phys. Rev. B* **77**, 195326 (2008).
- [46] S. Longhi and G. DellaValle, *Phys. Rev. A* **87**, 013634 (2013).
- [47] M. Grifoni and P. Hänggi, *Phys. Rep.* **304**, 229 (1998).
- [48] The renormalized tunneling rate can be set to be real and positive without loss of generality. Actually, for any complex value of Θ_0 , the phase transformation $C_{n,m} \rightarrow C_{n,m} \exp[i(n+m)\alpha]$, with α being the phase of Θ_0 , allows one to recast the coupled equations of the array with complex tunneling rate $\Theta_0\kappa$ into equivalent coupled equations with real tunneling rate $\kappa_e = |\Theta_0|\kappa$.
- [49] For a monochromatic driving field, surface defects could be, in principle, obtained by pushing the asymptotic analysis up to the order $\sim\epsilon^3$. This case, however, is not considered in our work because it would lead to a rather weak localization of the doublonic states. A bichromatic driving field enables a stronger localization, and therefore we limit here to consider this case.
- [50] For numerical computation of the energy spectra and eigenstates of the equivalent static lattice, we adopted a refined version of Eqs. (21), taking into account the effect of truncation of the semilattice, as detailed in Sec. IV B.
- [51] S. Wall, D. Brida, S. R. Clark, H. P. Ehrke, D. Jaksch, A. Ardavan, S. Bonora, H. Uemura, Y. Takahashi, T. Hasegawa, H. Okamoto, G. Cerullo, and A. Cavalleri, *Nat. Phys.* **7**, 114 (2011).
- [52] J. Schlappa, K. Wohlfeld, K. J. Zhou, M. Mourigal, M. W. Haverkort, V. N. Strocov, L. Hozoi, C. Monney, S. Nishimoto, S. Singh, A. Revcolevschi, J.-S. Caux, L. Patthey, H. M. Rønnow, J. van den Brink, and T. Schmitt, *Nature (London)* **485**, 82 (2012).
- [53] I. Bloch, J. Dalibard, and S. Nascimbene, *Nat. Phys.* **8**, 267 (2012).
- [54] G. Corrielli, A. Crespi, G. Della Valle, S. Longhi, and R. Osellame, *Nat. Comm.* **4**, 1555 (2013).